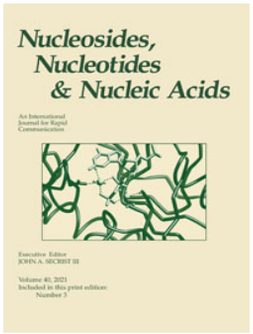

Nucleosides, Nucleotides & Nucleic Acids

ISSN: (Print) (Online) Journal homepage: https://www.tandfonline.com/loi/lncn20

Synthesis, characterization, ADMET, *in vitro* and *in vivo* studies of mixed ligand metal complexes from a curcumin Schiff base and lawsone

Porkodi Jeyaraman, Michael Samuel, Antonysamy Johnson & Natarajan Raman

To cite this article: Porkodi Jeyaraman, Michael Samuel, Antonysamy Johnson & Natarajan Raman (2021) Synthesis, characterization, ADMET, *in vitro* and *in vivo* studies of mixed ligand metal complexes from a curcumin Schiff base and lawsone, Nucleosides, Nucleotides & Nucleic Acids, 40:3, 242-263, DOI: 10.1080/15257770.2020.1867865

To link to this article: https://doi.org/10.1080/15257770.2020.1867865

Published online: 30 Dec 2020.

NUCLEOSIDES, NUCLEOTIDES AND NUCLEIC ACIDS
2021, VOL. 40, NO. 3, 242–263
https://doi.org/10.1080/15257770.2020.1867865

Taylor & Francis
Taylor & Francis Group

Synthesis, characterization, ADMET, *in vitro* and *in vivo* studies of mixed ligand metal complexes from a curcumin Schiff base and lawsone

Porkodi Jeyaraman[a], Michael Samuel[b], Antonysamy Johnson[c], and Natarajan Raman[b]

[a]Research Department of Chemistry, The Standard Fireworks Rajaratnam College for Women, Sivakasi, India; [b]Research Department of Chemistry, VHNSN College, Viruthunagar, India; [c]Department of Plant Biology and Plant Biotechnology, St. Xavier College, Palayamkottai, India

ABSTRACT

Complexes are currently synthesized from plant origin because of their therapeutic effect against certain diseases with toxicity. Hence, in this work, four new transition metal(II) mixed ligand complexes have been synthesized using a curcumin Schiff base (primary ligand) and lawsone (as co-ligand). The geometry of these complexes was explored by elemental analyses, molar conductance, thermal analysis, magnetic moment values, IR, NMR, Mass, electronic and EPR spectral studies. Electronic absorption titrations, viscosity measurements and molecular docking studies reveal that all the metal complexes interact with the CT DNA by groove binding. Among all the complexes, the copper(II) complex (complex 1) exhibits a higher K_b value (3.5×10^{-4} M) which reveals that it has a strong binding efficiency toward the CT DNA. The complexes also possess strong DNA cleavage efficiency. Cytotoxicity investigations on *Artemia salina* show that all the complexes possess higher cytotoxic effect than the ligand. Moreover, all the metal complexes have better antimicrobial efficacy than the ligand. Swiss ADME, PASS and pkCSM online softwares are helpful to predict the pharmacokinetic and biological actions of the curcumin Schiff base. Theoretical results obtained from the *in silico* study are experimentally corroborated by *in vivo* anti-inflammatory screening study. All the above studies demonstrate that the copper complex possesses biological activity similar to that of the drug like molecules.

RESEARCH HIGHLIGHTS

- Synthesis and characterization of four novel transition mixed ligand complexes using plant moieties
- Promising in *vivo* anti-inflammatory agents and *in vitro* DNA metallonucleases
- Cytotoxicity investigation on *Artemia salina*
- Higher cytotoxic effect for the complexes than the ligand
- Identification of copper(II) complex as lead like molecule among all

ARTICLE HISTORY
Received 7 January 2020
Accepted 19 December 2020

KEYWORDS
Lawsone; groove mode; cytotoxicity; in silico; anti-inflammatory

CONTACT Natarajan Raman ramchem1964@gmail.com Research Department of Chemistry, VHNSN College, Viruthunagar 626 001, India.

Supplemental data for this article can be accessed at https://doi.org/10.1080/15257770.2020.1867865.

GRAPHICAL ABSTRACT

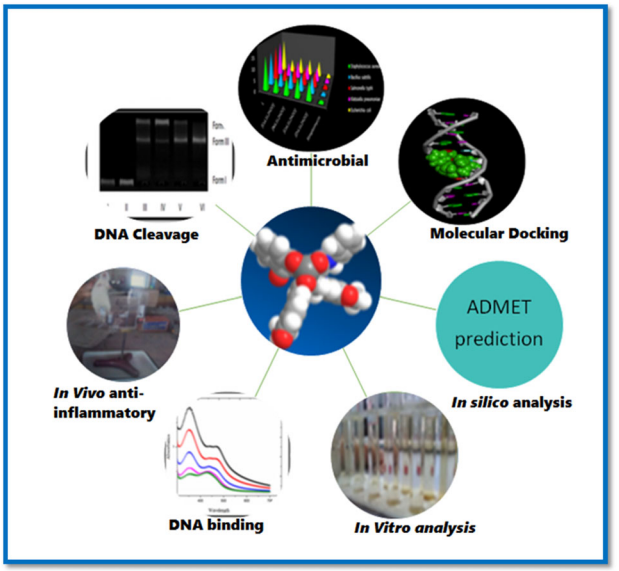

1. Introduction

At present, researchers are using phytochemicals derived from medicinal plants as new lead compounds. In recent medicinal research of new and efficient analogues from these phytochemicals have been investigated. Today, approximately 120 diverse chemical substances from plant origin are examined as potential candidates against many frightful diseases like HIV, cancer, malaria, inflammation *etc*.[1] Curcumin, a multipotent organic species considered as the Indian solid gold,[2] is obtained from *Curcuma longa*. Because of its hydrophobic nature, it exhibits poor pharmacokinetic behavior. This can be circumvented by complexation with various transition metal ions.[3] Due to the presence of the keto group, it can easily condense with a primary amine group and form Schiff base. The metal complexes from curcumin Schiff bases are found to have more therapeutic activity than free curcumin.[4–7]

Similarly, henna leaves are applied as a folk medicine (from the primordial period itself) to treat numerous diseases such as leprosy, small pox, chicken pox, HIV, cancer and tumors.[8–13] The chief bioactive material in this henna plant is lawsone (2-hydroxy-1,4-naphthoquinone), which is a bidentate ligand, able to coordinate with various metal ions and to increase its bio-activity.[14] Moreover, mixed ligand chelation due to its higher stability, forms easily inside the biological fluid membrane (because of the

Table 1. Physical and analytical data of the synthesized curcumin Schiff base and its complexes.

Compound	Yield (%)	Color	Calc (Found) %				Formula weight	Λ_m	μ_{eff} (BM)
			M	C	H	N			
$L_1(C_{32}H_{31}N_3O_6)$	80	Orange red	–	69.4 (70.1)	5.6 (5.6)	7.5 (7.6)	553	–	–
$[CuL_1L_2H_2O]$ (Complex 1)	75	Maroon	7.9 (7.8)	62.5 (62.4)	4.6 (4.6)	5.2 (5.1)	807	7	1.82
$[CoL_1L_2H_2O]$ (Complex 2)	66	Dark brown	7.3 (7.2)	62.8 (62.7)	4.7 (4.8)	5.2 (5.1)	802	6	4.21
$[NiL_1L_2H_2O]$ (Complex 3)	64	Yellowish brown	7.3 (7.2)	62.8 (62.7)	4.6 (4.6)	5.2 (5.3)	802	6	3.10
$[ZnL_1L_2H_2O]$ (Complex 4)	61	Orange red	8.1 (8.1)	62.4 (62.3)	4.6 (4.6)	5.2 (5.1)	809	5	Dia Magnetic

Unit of Λ_m = ohm^{-1} cm^2 mol^{-1}.

presence of bioactive ligands). They compete with metal ions *in vivo*[15] and also act as store house and mediator of several active materials through the biological membranes.[16,17] They attain more biological activity than the homo ligand complexes. Both the curcumin and lawsone metal complexes are individually examined for DNA binding and cleavage efficiency, protein targeting, antioxidant, tumor inhibition and cytotoxic activities *etc.*[18–22] Before going for blind *in vivo* study, *in silico* screening study in medicinal chemistry provides a tempo for the detection of drug like compounds and it also helps to ease the usage of expensive lab work and clinical trials.[23]

In light of the above facts, the current research work deals with the synthesis of transition mixed ligand complexes from curcumin Schiff base and lawsone (co-ligand). They have been characterized by UV-Vis, FT-IR, NMR, EPR, mass and TGA analytical techniques. All the synthesized compounds were investigated for DNA binding efficacy by adopting electronic absorption titrations, viscosity measurements and molecular docking techniques. Moreover, all the synthesized compounds were examined for DNA nuclease activity. Pharmacokinetic behavior of the ligand was also evaluated by pkCSM and SWISS ADME tools. As per the PASS online data of the curcumin Schiff base ligand from our previous research work,[24] all the metal complexes were analyzed for *in vivo* anti-inflammatory activity. Cytotoxicity and antimicrobial activities of the ligand and metal complexes were also inspected.

2. Experimental

The supplementary file S1 provides the instrumental details, investigational procedures for the DNA binding and cleavage studies, *in vitro* antimicrobial screening, cytotoxic analysis, *in silico* and *in vitro* anti-inflammatory screening studies.

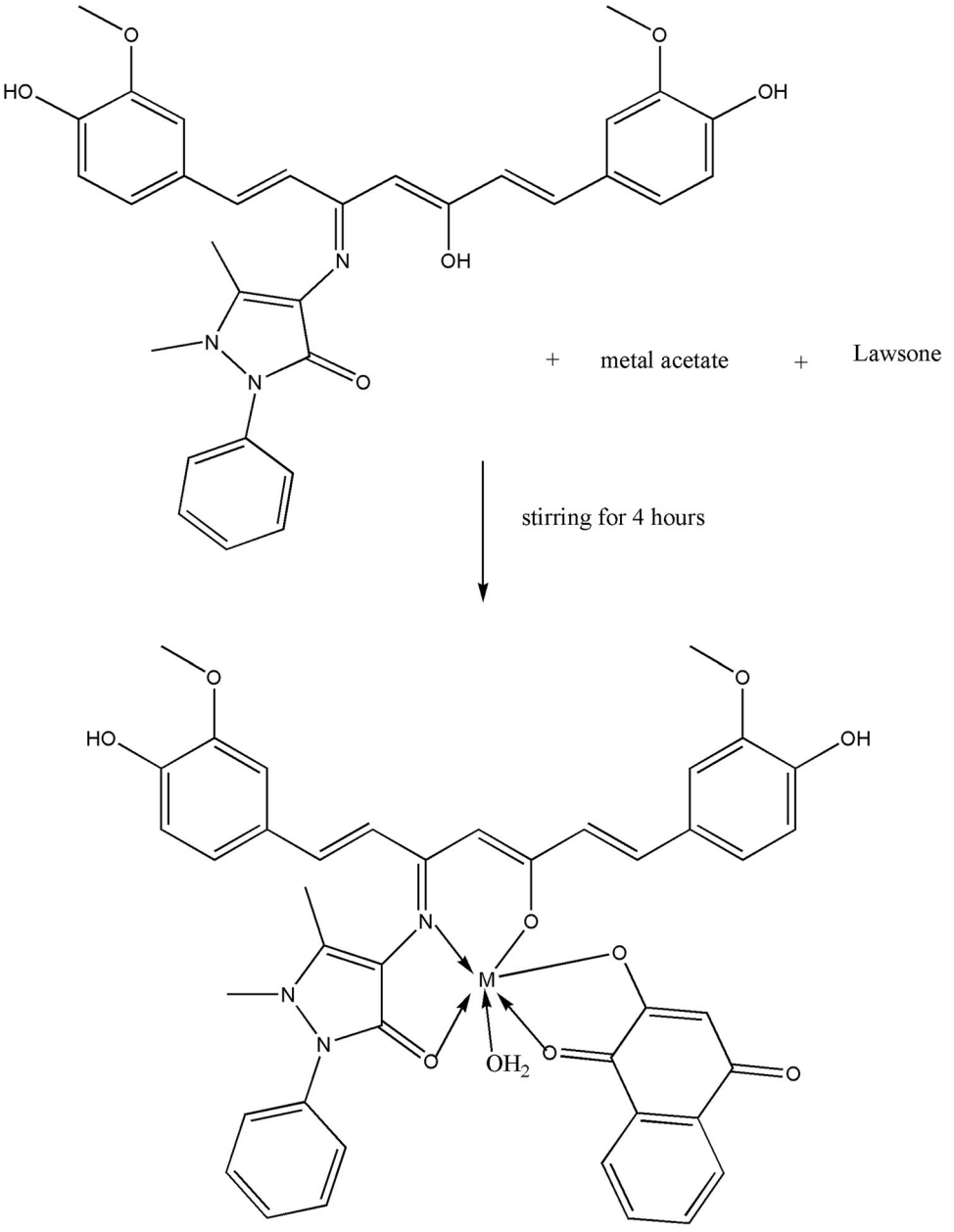

$\mathbf{M = Cu^{2+}, Co^{2+}, Ni^{2+}, Zn^{2+}}$

Scheme 1. Schematic route for the synthesis of metal complexes using curcumin Schiff base (L_1) and the co-ligand lawsone (L_2).

2.1. Synthesis of mixed ligand metal complexes

As per the literature survey, the curcumin Schiff base ligand (L_1) was synthesized.[24] Equimolar proportion of L_1 and metal(II) acetate [Cu(II)/

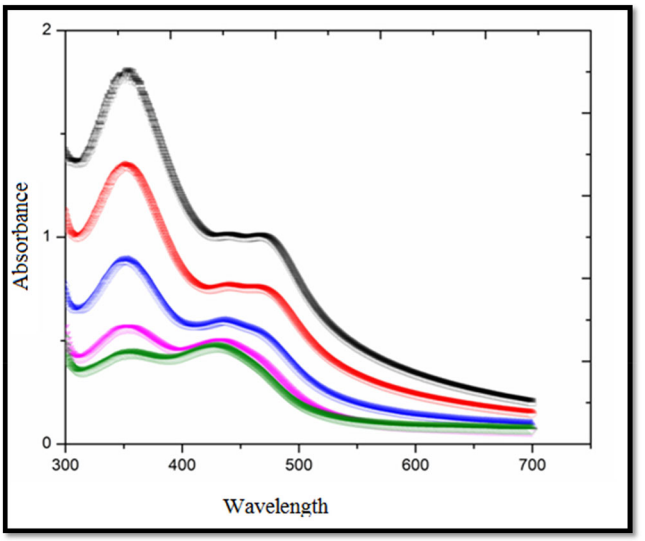

Figure 1. The absorption spectra of the complex 2 in buffer pH =7.2 at 250 C in presence of increasing amount of DNA.

Ni(II)/Co(II)/Zn(II)] was dissolved in methanol and stirred for *ca* 30 min. To this mixture, same concentration of lawsone (L_2) was added and the whole mixture was stirred for 4 h. The obtained solid mass was recrystallized using ethanol. The schematic route for the synthesis of metal complexes using curcumin Schiff base (L_1) and the co-ligand lawsone (L_2) was given in Scheme 1.

3. Results and discussion

The synthesized metal complexes are easily soluble only in DMF and DMSO solvents. Due to amorphous nature of metal complexes, no single crystal, suitable for X-ray determination could be isolated.

3.1. Elemental analysis and molar conductance

The physical and analytical values for the stable ligand L_1 and its complexes [Cu(II) complex (1); Co(II) complex(2); Ni(II) complex (3); Zn(II) complex (4)] are given in Table 1. This is evident for $ML_1L_2H_2O$, metal-ligand stoichiometry. The molar conductance values were noticed in the range of 5–7 ohm^{-1} cm^2 mol^{-1}. These values reveal the non- electrolytic nature of metal complexes.[25,26]

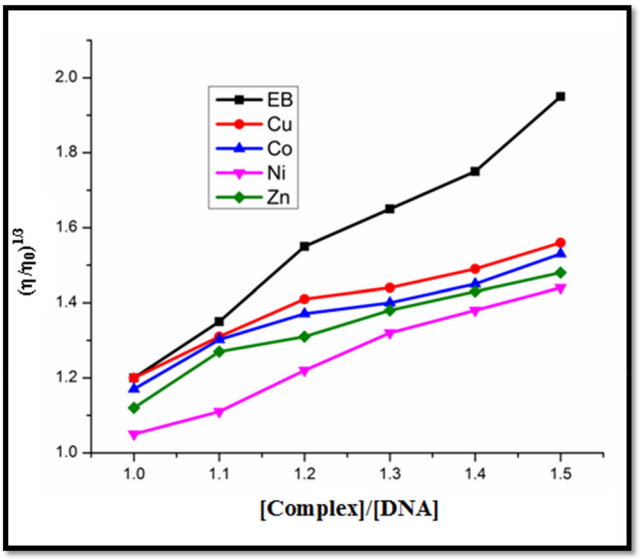

Figure 2. Effect of increasing amount of EB] (■), Complexes 1 (●), 2 (♦), 3 (▼) and 4 (▲) on the relative viscosity of CT DNA. Plot of relative viscosity $(\eta/\eta o)^{1/3}$ *vs* [complex]/[DNA].

3.2. Electronic absorption spectra and magnetic moments

From the UV-Vis absorption data, geometry of the complexes was assigned. Two intense absorption bands were exhibited by the ligand (in DMSO solvent) at 266 nm (37,594 cm^{-1}) and 434 nm (23,041 cm^{-1}) which are due to $\pi \rightarrow \pi^*$ and $n \rightarrow \pi^*$ transitions.

An absorption band at 14,136 cm^{-1} was shown by the complex 1 which is due to $^2E_g \rightarrow {}^2T_{2g}$ transition (Figure S1). The magnetic moment value for this complex 1 is 1.82 BM. The above data corroborate the octahedral geometry and the existence of one unpaired electron in its d-orbital.[27] Likewise, the octahedral geometry for the complex 2 is confirmed by the three absorption bands at 12,549, 22,732 and 18,221 cm^{-1} which are due to $^4T_{1g}(F) \rightarrow {}^4T_{2g}(F)$, $^4T1g\ (F) \rightarrow {}^4A2g(F)$ and $^4T1g\ (F) \rightarrow {}^4T1g(P)$ transitions and 4.21 BM magnetic moment value. The mononuclear complex 3 with octahedral geometry[28] is also confirmed by three low intensity bands *viz.*, 12,919, 21,458 and 17,609 cm^{-1} and 3.10 BM magnetic moment value.

Due to the diamagnetic nature of complex 4, only ligand to metal charge transfer transition absorption band is obtained at 25,778 cm^{-1} and it also possess zero magnetic moment. Therefore, for the complex 4, only the elemental analysis and other analytical data, its geometry can be predicted which also shows that it possesses an octahedral geometry.[29]

3.3. FT-IR spectral study

The coordination sites present between the ligand and metal complexes can be found out with the help of FT–IR spectrum. Usually, the stretching

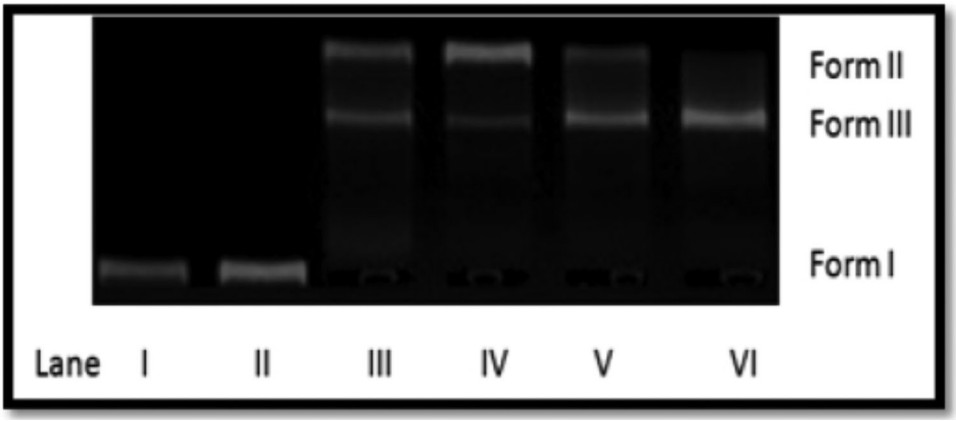

Figure 3. Gel electrophoresis template showing the cleavage of pUC19 DNA treated with metal complexes: Lane I: DNA control; Lane II: DNA + L1+ H_2O_2; Lane III: DNA + complex 1 + H_2O_2; Lane IV: DNA + complex 3 + H_2O_2; Lane V: DNA + complex 2 + H_2O_2 and Lane VI: DNA + complex 4 + H_2O_2.

frequencies for the corresponding coordinating sites present in the ligand get decrease or increase after the metal complexation.[30] The stretching bands at 1627 cm^{-1} and 1597 cm^{-1} are due to C = O and C = N functional groups present in the ligand L_1. Lawsone (the co-ligand L_2) exhibits C = O stretching at 1678 cm^{-1} (chelated) and 1648 cm^{-1} (unchelated) respectively. These stretching frequencies are shifted to lower values after complexation around 1610–1620 cm^{-1} and 1641–1649 cm^{-1} for the C = O functional group in ligands L_1 and L_2 in all the complexes. Also C = N functional group stretching frequency value for all the complexes is also shifted to lower value around 1561–1575 cm^{-1}. This shifts make an evidence for the complexation of C = O from both ligands and C = N from L_1 with metal ions.

The stretching frequencies for C = O and -C = N functional groups get decrease after the coordination with metal ion. Moreover, many new bands are appeared in the range of 507–513 cm^{-1}, 424–429 cm^{-1} and 615–618 cm^{-1} in all the metal complexes (except the ligands) which reveal the presence of new M-O and M-N bonds (in L_1)[31] and M-O bond (in L_2),[32] respectively (Figure S2).

3.4. Nuclear magnetic resonance spectroscopy

Using DMSO-d_6 solvent, the NMR spectra of the ligands and Zn(II) complex were recorded. The singlet peaks obtained in the proton NMR at 12.8 ppm and 11.66 ppm[33] for the ligand L_1 and L_2 are due to the enolic OH proton in ligand L_1 and the OH proton in ligand L_2. These singlet peaks get vanished after complexation with the metal ion. It is observed

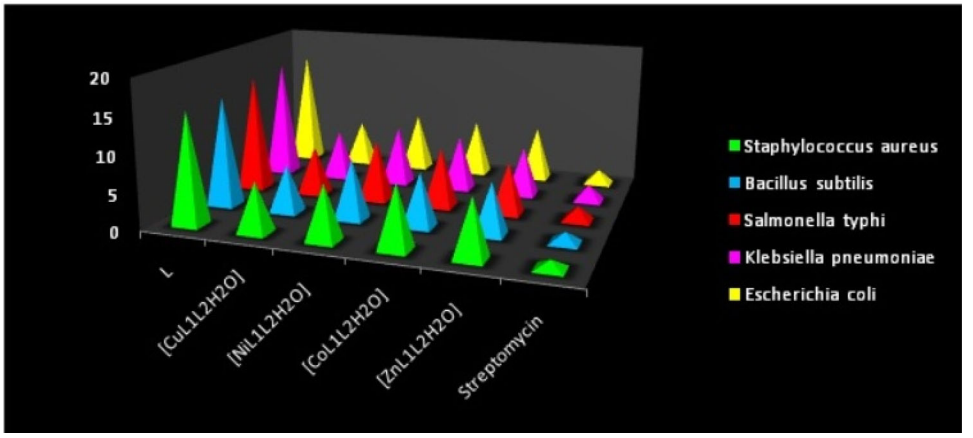

Figure 4. Antibacterial activity of synthesized complexes.

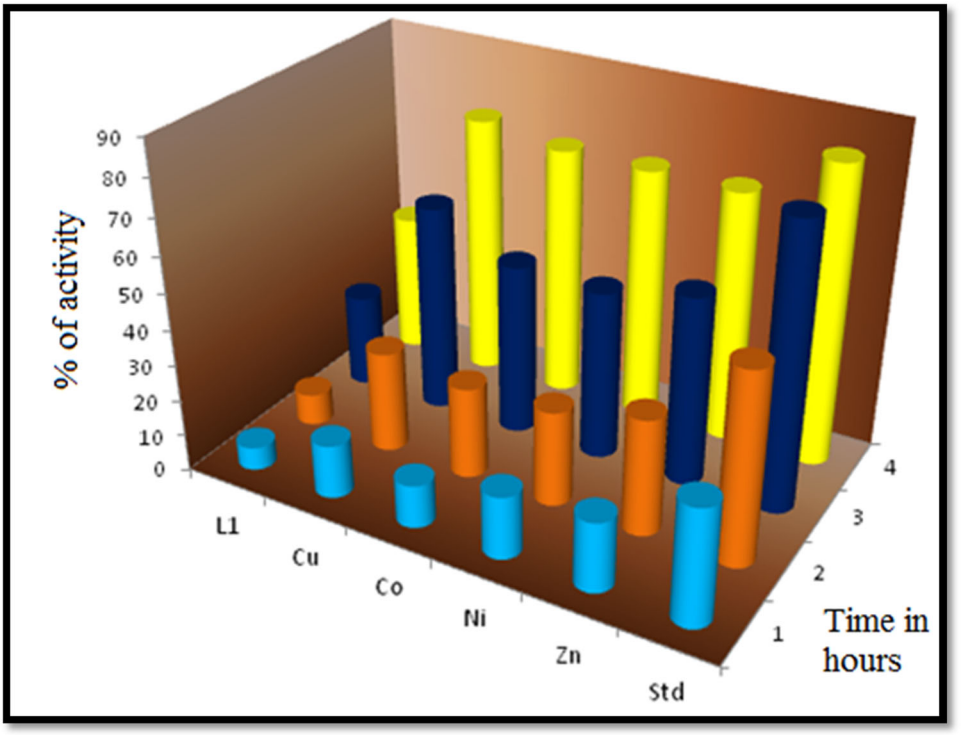

Figure 5. Anti-inflammatory activity of ligand and metal complexes.

from the proton NMR spectrum of the complex 4 (Figure S3). This corroborates the linkage of both OH groups with the Zn(II) complex.

The ligand L_1 displays signals at 124–138 ppm, 148 ppm and 183 ppm in ^{13}C NMR which are due to aromatic carbon, C = N carbon and C = O carbon respectively. After coordination with Zn(II) complex the C = N and C = O carbon peaks in ligand L_1 are also shifted to upfield at 141 ppm and

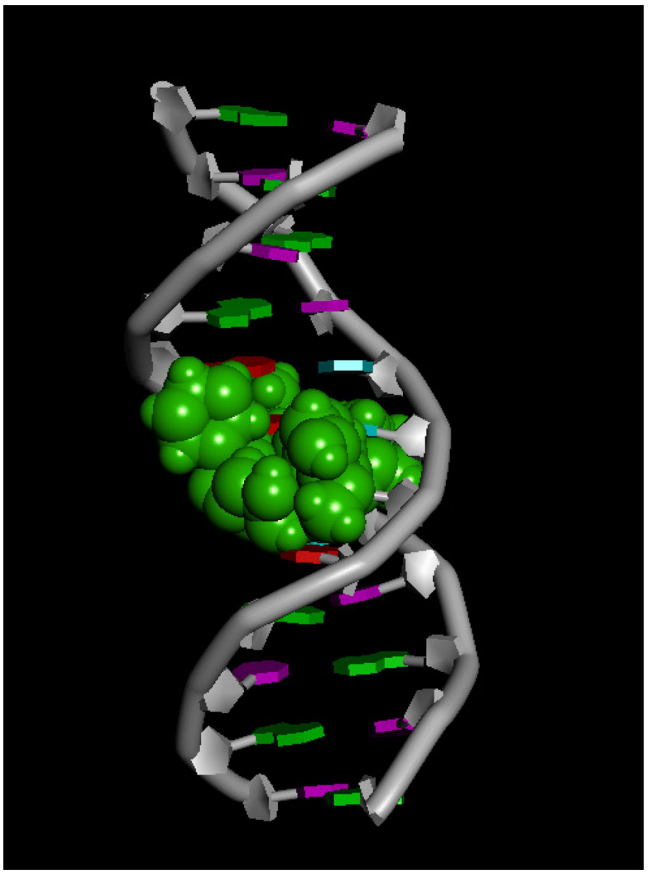

Figure 6. Docking of zinc complex with 1BNA.

171 ppm. This is also seen in the ligand L_2 whose carbon peak observed at 188 ppm and it is due to the C = O functional group (Figure S4). It is also shifted to upfield after complexation at 182 ppm. The above ^{13}C NMR data reveal the complexation of C = O functional group from both ligands and C = N moiety from ligand L_1 with complex 4.

3.5. Mass spectra

The assigned stoichiometry of the synthesized complexes was confirmed by the ESI-Mass data. The Figure S5 shows the ESI mass spectrum of the complex 1. The ligand exhibits a M^+ and fragmentation peaks at m/z = 553.3 and 450, 301 and 235, which are equivalent to the stoichiometry of ligand L_1 and the formation of $[C_7H_8N_2]^+$, $[C_{14}H_{11}N_3O_2]^+$ and $[C_{13}H_{17}NO_3]^+$ fragments respectively. The complex 1 displays its $[M^+]$ peak at m/z = 807 which is corresponding to the molecular weight of the complex and molecular formula $[CuC_{42}H_{37}N_3O_{10}]$. Moreover, the

Table 2. The spin Hamiltonian parameters of the complex 1 in DMSO solution.

	g-tensor			$A \times 10^{-4}$ (cm^{-1})				
Complex	$g_{\|\|}$	$g_{\perp}$	g_{iso}	$A_{\|\|}$	$A_{\perp}$	A_{iso}	$g_{\|\|}/A_{\|\|}$	G
Complex 1	2.278	2.06	2.15	170.5	51	132.5	133	4.63

fragmentation peaks are noticed at m/z 738.97, 485.98 and 429.96 which are due to development of the species $[CuC_{36}H_{30}NO_{11}]^+$, $[CuC_{21}H_{21}N_1O_7]^+$ and $[CuC_{21}H_{20}O_6]^+$ respectively. These mass spectral data also confirm the formation of metal complexes of $[ML_1L_2H_2O]$.

The diverse M^+ peaks emerged in these spectra of the complexes are ascribed to the breakup of the different bonds in metal complex within the molecule. The mass spectrum of complex 1 shows a variety of peaks which are in burly accord with the proposed structure by elemental analyses, spectral and magnetic moment studies.

3.6. EPR spectra

The EPR spectra of paramagnetic species render details regarding the bonding environment flanked by the ligand and metal center, geometry. This also provides detail on the distribution of unpaired electrons in the sub-orbitals. Four determined peaks in low field and one deep peak in the high field region are observed in the X- band EPR spectra of complex 1 which are taken both at 77 K and 298 K. This is primarily owing to the coupling of the electron spin ^{63}Cu nucleus (I = 3/2). The EPR spectrum of complex 1 is shown in Figure S6. The Table 2 displays the spin Hamiltonian factor of complex 1.

The magnetic susceptibility value of the complex 1 is 1.82 BM which is due to the presence of one paramagnetic electron. This shows that, there is no copper – copper interface in the complex 1 and there is no band at 1600 G due to $m_s = \pm 2$ transition. The complex 1 exhibits $g_{||}$ value at 2.278 and the $g_{\perp}$ value at 2.06.

$A_{||}$ (170.5) > $A_{\perp}$ (51), g-tensor values ($g_{||} > g_{\perp}$) and G value for complex 1 authenticate the existence of $d_{x^2-y^2}$ as the ground state and the octahedral geometry of this complex.[34] This complex has G value of 4.63, which strongly evident for parallel or somewhat distorted arrangement of the neighbor tetragonal axes.[35] Moreover, the covalent nature of the metal-ligand bond is predicted by the $g_{||}$ value of the metal complex. If the $g_{||}$ is higher than 2.3, then the metal-ligand bond is ionic in nature and if it is lower, then the bond is covalent character in nature.[36] The observed $g_{||}$ for complex 1 is lower than 2.3 which shows the copper complex is covalent in nature, which confirms the existence of copper–nitrogen bonds in this chelate. The value of $g_{||}/A_{||}$ is 133 cm^{-1} which also shows that complex 1 has distorted octahedral geometry. Thus, these EPR data give a

Table 3. Electronic absorption parameters for the interaction of DNA with synthesized metal complexes in 10-4 M solution.

Compound	λ max(nm)		Δλ		
	Free	Bound	(nm)	[a]H%	$K_b \times 10^4$ (M^{-1})
Complex 1	349	360	11	3.15	3.5
Complex 2	356	361	5	1.40	1.8
Complex 3	357	365	8	2.24	2.8
Complex 4	350	355	5	1.43	3.1

[a]$H\% = [(A_{free} - A_{bound}) / A_{free}] \times 100\%$.

supportive proof to the UV-Visible spectra and magnetic susceptibility value in predicting the geometry of the metal complexes.

3.7. Thermal studies

This technique is widely used to study coordinated water molecule. The existence of one water molecule inside the coordination sphere is in concert with the elemental analysis which is presented in Table 1. The result of the thermogravimetric analyses of the cobalt complex measured from ambient temperature upto 1000 °C at a heating range of 10 °C min^{-1} under nitrogen atmosphere is discussed in details. TGA and DTA analyses of complex 2 are given in Figures S7 and S8. The weight reduction has been estimated from the encompassing temperature upto 1000 °C.

Thermogram of complex 2 shows 95% weight reduction above 900 °C which is seen in the subsequent steps *viz*., (i) 30% reduction in weight is noticed in 176–300 °C temperature which is due to removal of coordinated water and then a steady weight reduction in the range of 300–440 °C and 440–600 °C which can be occurred because of whole disintegration of 4-aminoantipyrine ligand and lawsone co-ligand inside the metal complex.[24] Finally, the complex 2 is charred and transformed into its metal oxide. Furthermore, the existence of coordinated water in sixth position is affirmed by the endothermic peaks, seen in DTA curve in 176–300 °C temperature.

3.8. DNA binding studies

3.8.1. UV spectral titrations

There has been an escalating study on the nature of bonding existing between the DNA and different molecules which is useful to comprehend the mechanism of action of many DNA and noxious attacking drugs.[37] The fastening action of all the complexes is explored by absorption spectral titration. The UV spectral titration of complex 3 in the existence and non-existence of CT DNA is given in Figure 1.

During the course of the titration, there is a gradual increase in the concentration of the CT DNA which affects the absorption spectra of the

Table 4. Minimum inhibitory concentration of the synthesized ligand and metal complexes against the growth of bacteria (μM).

	MIC values ($\times 10^4$μM) SEM = ±1.2				
Compound	*Staphylococcus aureus*	*Bacillus subtilis*	*Salmonella Typhi*	*Klebsiella pneumoniae*	*Escherichia coli*
L_1	15.3	15.1	16.2	16.5	16.2
Complex 1	6.8	6.5	6.7	6.8	6.2
Complex 2	8.5	7.3	8.2	7.6	7.7
Complex 3	7.5	8.2	8.4	8.2	8.0
Complex 4	7.9	7.0	7.1	6.8	7.5
Streptomycin	1.2	1.5	2.0	2.3	2.0

complex. Hypochromism and a slight red shift are noticed in all the metal complexes. This is because of the tightening of DNA in the helix axis and change in the conformation of DNA.[38] Intensive absorption spectrum with maxima at 349 nm, 357 nm, 356 nm and 350 nm are seen for the complexes 1, 2, 3, and 4 respectively in Tris-HCl buffer solution. These are produced because of intra-ligand π-π* transition. The intensity of absorption band increases with increase in the concentration of CT DNA which promotes hypochromicity and a minor bathochromic shift. These changes indicate the groove/surface mode of interaction existed between the complexes and CT DNA like distamycin, mitomycin, netripsin and spermine.[39]

Table 3 displays the DNA binding constant results of the synthesized metal complexes. The graph between $[DNA]/[\varepsilon_a - \varepsilon_f]$ *vs* [DNA] provides slope and intercept data, from which the binding constant values are determined. The binding competency of the metal complexes is in the subsequent order:

$$\text{Complex 1} > \text{Complex 2} > \text{Complex 3} > \text{Complex 4}$$

The complex 1 has stronger DNA binding activity toward the CT DNA than other complexes because of its higher K_b value (3.5×10^{-4} M^{-1}).

3.9. Viscosity measurements

Viscosity measurement also provides an additional evidence to investigate the mode of binding interface between the synthesized complexes and CT DNA. Here, the concentration of the metal complexes is altered and the comparative viscosity of the CT DNA is recorded. Without XRD data, the most critical tests for DNA binding are the hydrodynamic methods which are very responsive to change in the length of the DNA. A conventional intercalator after binding with the CT DNA increases its viscosity by broadening of base pairs in the DNA helix. But an unfair or non-conventional intercalator decreases the effective length of DNA helix and its viscosity.[40,41] Due to the bulky nature of the synthesized complexes, surface binding with CT DNA takes place which decreases the relative viscosity.

Table 5. Minimum inhibitory concentration of the synthesized ligand and metal complexes against the growth of fungi (μM).

	MIC values ($\times 10^{-4}$ μM) SEM = ±1.0				
Compound	*Aspergillus niger*	*A.flavus*	*Curvularia lunata*	*Rhizoctonia bataticola*	*Candida albicans*
L_1	22.5	23.0	23.6	23.2	24.5
Complex 1	14.5	14.1	14.6	14.5	13.5
Complex 2	16.5	17.4	16.6	16.2	16.0
Complex 3	17.5	17.9	17.1	17.6	17.6
Complex 4	15.9	15.5	15.7	14.9	14.6
Clotrimazole	3.5	3.7	4.2	4.0	4.5

Amid all complexes, complex 1 has more potential toward DNA binding. Figure 2 shows the viscosity of CT DNA with the synthesized compounds and ethidium bromide.

3.10. DNA cleavage study

Denaturation of DNA can be inhibited by numerous methods and procedures. One among is scissoring of supercoiled DNA using various lead like molecules by undergoing oxidative or hydrolytic cleavage. Like enzymatic cleavage, oxidative and hydrolytic cleavages destruct the sugar components and phosphodiester linkages. They are the backbone of the DNA.

During this strategy, the quickest cleavage is the form I which is the supercoiled phase. After this cleavage, a moderate loosen up cleavage of form II (nicked phase) is created. Stage III is linear phase produced at the last.[42] Figure 3 obviously investigates that all the synthesized complexes have the strong capacity to cleave the plasmid DNA because of the addition of H_2O_2. The hydroxyl or super oxide free radical formed after reaction with metal complexes assists in the oxidation process and causes the incision of pUC19 DNA.

Lane I and lane II, do not exhibit any considerable incision of pUC19 DNA. Complex 4 cuts the pUC19 DNA into open circular form I which is clearly found in lane IV, but the other three complexes break the pUC19 DNA into nicked and horizontal forms. This study clearly exposes the potential of synthesized complexes in the cleavage of pUC19 DNA.

3.11. Antimicrobial screening

Antimicrobial examination was done by adopting broth dilution method. All the compounds were analyzed against *Staphylococcus aureus*, *Bacillus subtilis*, *Salmonella typhus*, *Klebsiella pneumoniae* and *E. coli* bacteria and some dissimilar strains of fungi like A. *flavus, Aspergillus niger*, *Curvularia lunata, Candida albicans* and *Rhizoctonia bataticola.*

Table 6. Cytotoxic bioassay data of the synthesized compounds.

S.No	Compounds	LC_{75} (M/mL)
1.	Ligand L_1	3.181×10^{-4}
2.	Complex 1	1.135×10^{-4}
3.	Complex 2	1.867×10^{-4}
4.	Complex 3	1.588×10^{-4}
5.	Complex 4	1.167×10^{-4}

The MIC (Minimum Inhibitory Concentration) values are tabulated in Tables 4 and 5 which reveal that the complex 1 possesses higher antimicrobial activity than the other compounds.

Figure 4 also reveals the higher antimicrobial efficiency of complexes when compared to ligand L_1. This is because of the co-ordination of ligands with the metal ions which causes the hindering of the protein synthesis of bacteria and fungi and prohibits their growth and multiplication. This chelation effect diminishes the ionic character of metal ion.[43]

The lipids and polysaccharides compounds found inside the cell membranes have constructive sites for binding with metal ions. Interestingly, the liphophilic complexes encourage their diffusion into the lipid membrane and stop the enzymatic action of the micro organisms. This enhancement is also pronounced by the nature and geometry of metal complexes and its ADMET property.

3.12. ADMET prediction

Because of poor pharmacokinetic ADMET property, majority of the lead like molecules fails in the clinical trials. *In silico* examination helps in drug design development before lead like molecules entering into the preclinical phases and thus save the cost and time. The pharmacokinetic behavior of the curcumin Schiff base has been examined by SWISS ADME and pkCSM online softwares. These outputs from both the softwares can be evaluated with the help of Lipinski' rule of five.[44] The ligand L_1 has the ability to penetrate into the biological membrane because its calculated log p value is 4.86 (less than 5) in SWISS ADME software. The ligand L_1 has 118 A^0 (below 140 A^0) TPSA value (total polar surface area), 3 hydrogen bond donors and 3 hydrogen bond acceptors (which are also less than 5 and 10) and 9 rotatable bonds ($\leq$10 according to Veber's rule).[45] These data imply the efficient transport of it by oral method and also inside the GIT (Gastro Intestinal Tract) and BBB (Blood Brain Barrier). The bioavailability score is 0.55 ($>$ than 0) which also reveals that the curcumin Schiff base is a biologically active one.

Similarly, the ADMET property analyzed by the pkCSM software reveals that it has 95.64% ability to undergo absorption inside the human GIT. The log K_p value of the ligand L_1 is -2.735 (which is less than $-$ 2.5)

which indicates that it can penetrate into the skin. VDss value denotes the theoretical volume of drug distributed evenly in the blood plasma and the ligand L_1 has the VDss value −0.364 which is relatively less than the standard value − 0.15. This shows that the ligand is distributed more in blood plasma and less in tissue and therefore no renal failure and dehydration is caused. It is metabolized by CYP3A4 substrate, CYP2C19 inhibitor and CYP3A4 inhibitor enzymes. These enzymes render oxidation process and facilitate their excretion. It has nontoxic value and non–carcinogen in nature.[46]

3.13. Anti-inflammatory examination using albino rats

Our previous report shows that the metal complexes exhibit higher anti-inflammatory activity than ligand L_1.[24] After considering the p_a value obtained from the PASS biological activity prediction software, all the synthesized compounds have been examined for *in vivo* anti-inflammatory action by adopting carragenan stimulated mice paw edema inhibition technique using ibuprofen as reference drug and felbinac as parent drug. This method encompasses the biphasic stages and various mediators take part in the inflammatory reaction evoked by carrageenan. The primary stage of the inflammatory reaction is due to the liberation of histamine and 5-hydroxytryptamine almost for 90 min. Then for 2.5 h, kinin-mediated increased vascular permeability takes place. Neutrophil infiltration and release of prostaglandins and prostaglandin-connected leukocytes into the location of edema take place at the last stage nearly for 3.5 h which makes the feet swiftly swollen. It is investigated that the anti–inflammatory action of the ligand L_1 has been increased after complex formation which is shown in the graphical diagram (Figure 5).

Among all the tested compounds, complex 1 exhibits 80.1% of anti-inflammatory activity and it is prominent to be significantly more potent than felbinac (62.44%) but quite similar to clinically used drug ibuprofen (81.5%). Due to liphophilic nature of complexes, penetration into the cell membranes becomes an easier one and they have potent to hinder cyclooxygenase synthesis.[47–50] Moreover, the metal complexes derived from lawsone possess higher anti-inflammatory than the complexes derived from flavonoid (quercetin). This is due to the planarity and less steric effect of the lawsone moiety.

3.14. In vitro cytotoxic analysis

Brine shrimp lethality assay has been widely used as one of the best bioassays for the detection and refining of biologically active compound.[51]

Brine shrimp, *Artemia* species are particularly termed as sea monkeys. This study generally deals on the tendency of the compounds to kill the laboratory-cultured *Artemia nauplii* brine shrimp. Cytotoxicity activity of the synthesized compounds is analyzed by using Meyer et al., protocol.[52] Median lethal concentrations of all the compounds have been obtained from the plot between percentage of mortality and the concentration of the screened compounds.

Table 6 clearly indicates that the complexes possess higher cytotoxicity efficiency than the ligand L_1. Among all, complexes 1 and 4 have significant cytotoxicity activity with LC_{75} values, 1.135×10^{-4} and 1.167×10^{-4} M/mL respectively.

4. Molecular docking

Computational methods such as molecular docking are very helpful and sensibly reliable for prediction of recognized binding modes and affinities of ligands for macromolecules.[53] Lowering the binding free energy value results higher binding affinity between the receptor and synthesized compounds. The binding constant values K_b undoubtedly point out the binding action of complexes with the DNA. The possibility of intercalation for the synthesized complexes is found to be less with DNA because of a smaller amount of effective stacking forces existing between curcumin moiety and DNA. The metal complexes associated with the curcumin moieties provide them more H-bond donor/acceptor atoms and hence facilitate them to reside in the minor groove by means of van der Wall's forces and hydrogen bonds.

The energy minimized docking results reveal the binding of complex inside DNA minor groove. In the current research work, all the synthesized compounds are docked into the cancer DNA (PDB ID: BNA) efficiently *via* groove mode (which is shown in Figure 6).

The binding energies of docked compounds are found to be −344.63 (L_1), −362.35 (complex 1), −353.37 (complex 2), −357.67 (complex 3) and −349.18 (complex 4) kJ mol^{-1} respectively. Besides van der Waal's interactions, all the metal complexes form one or more hydrogen bonds with base pairs and PO_2 group of DNA. The more the negative score, the more potent binding is existing between the DNA and target molecules.

5. Conclusion

In the current research work, four new mixed ligand complexes having lawsone as co-ligand have been synthesized. Using IR and NMR spectral studies, the functional groups involved in complexation from ligands L_1 are confirmed. By evaluating the data from elemental analysis, magnetic

moments, EPR, Mass and TGA studies elemental analysis, an octahedral geometry of the metal complexes is confirmed. UV-Visible titrations, viscosity measurements and molecular docking reveal the groove mode of binding which exists between the CT DNA and metal complexes. All the metal complexes (except complex 4) have higher efficiency to cleave plasmid DNA. ADMET property of the ligand L_1 has been examined by pkCSM and SWISS ADME online softwares. This *in silico* study reveals that the ligand L_1 is a biological active compound. As per the PASS online software data, *in vivo* anti-inflammatory screening is inspected which shows that metal complexes exhibit higher anti-inflammatory action than ligand L_1. Moreover, complex 1 has anti-inflammatory activity similar to that of the standard. Cytotoxicity analysis and antimicrobial studies also confirm the higher biological character of the synthesized metal complexes. Comparing all the compounds, the complex 1 exhibits higher biological activity than the other complexes.

List of abbreviations

DNA	Deoxyribo Nucleic Acid
CT DNA	Calf Thymus Deoxyribo Nucleic Acid
UV-Vis	Ultra Violet – Visible spectroscopy
FT-IR	Fourier Transform – Infra Red
NMR	Nuclear Magnetic Resonance
EPR	Electron Paramagnetic Resonance
TGA	Thermo Gravimetric Analysis
DTA	Differential Thermal Analysis
ADMET	Adsorption, Distribution, Metabolism, Excretion, Toxicity
PASS	Prediction of Activity Spectra for Substances
pkCSM	Predicting small-molecule pharmacokinetic and toxicity properties
HIV	Human Immunodeficiency Virus
DMF	Dimethylformamide
DMSO	Dimethylsulfoxide
pUC	Plasmid University of California
GIT	Gastro-Intestinal Tract
BBB	Blood Brain Barrier
VDss	Volume of Distribution at steady state
CYP	Cytochrome P450 3A4
H- bonds	Hydrogen bonds
P_a	Probability of active

Acknowledgements

The authors express their heartfelt thanks to the College Managing Board, Principal and Head of the Department of Chemistry, VHNSN College (Autonomous), Virudhunagar for providing research facilities.

References

[1] Balunas, M. J.; Kinghorn, A. D. Drug Discovery from Medicinal Plants. *Life Sci.* **2005**, *78*, 431–441. DOI: 10.1016/j.lfs.2005.09.012.

[2] Shakeri, A.; Panahi, Y.; Johnston, T. P.; Sahebkar, A. Biological Properties of Metal Complexes of Curcumin. *Biofactors* **2019**, *45*, 304–317. DOI: 10.1002/biof.1504.

[3] Sareen, R.; Jain, N.; Dhar, K. L. Curcumin-Zn(II) Complex for Enhanced Solubility and Stability: An Approach for Improved Delivery and Pharmacodynamic Effects. *Pharm. Dev. Technol.* **2016**, *21*, 630–635. DOI: 10.3109/10837450.2015.1041042.

[4] Pallikkavil, R.; Ummathur, M. B.; Sreedharan, S.; Krishnankutty, K. Synthesis, Characterization and Antimicrobial Studies of Cd(II), Hg(II), Pb(II), Sn(II) and Ca(II) Complexes of Curcumin. *Main Group Met. Chem.* **2013**, *36*, 123–127. DOI: 10.1515/mgmc-2013-0023..

[5] Subhan, M. A.; Alam, K.; Rahaman, M. S.; Rahman, M. A.; Awal, R. Synthesis and Characterization of Metal Complexes Containing Curcumin ($C_{21}H_{20}O_6$) and Study of Their anti-Microbial Activities and DNA Binding Properties. *J. Sci. Res.* **2014**, *6*, 97–109. DOI: 10.3329/jsr.v6i1.15381.

[6] Joseph, J.; BoomadeviJanaki, G. Synthesis, Structural Characterization and Biological Studies of Copper Complexes with 2-Aminobenzothiazole Derivatives. *J. Mater. Environ. Sci.* **2014**, *5*, 693–704.

[7] Padhye, S.; Yang, H.; Jamadar, A.; Cindy Cui, Q.; Chavan, D.; Dominiak, K.; McKinney, J.; Banerjee, S.; Ping Dou, Q.; Sarkar, F. H. New Difluoro Knoevenagel Condensates of Curcumin, Their Schiff Bases and Copper Complexes as Proteasome Inhibitors and Apoptosis Inducers in Cancer Cells. *Pharm. Res.* **2009**, *26*, 1874–1880. https://dx.doi.org/10.1007%2Fs11095-009-9900-8. DOI: 10.1007/s11095-009-9900-8.

[8] Nittayananta, W.; Pangsomboon, K.; Panichayupakaranant, P.; Chanowanna, N.; Chelae, S.; Vuddhakul, V.; Sukhumungoon, P.; Pruphetkaew, N. Effects of Lawsone Methyl Ether Mouthwash on Oral Candida in HIV-Infected Subjects and Subjects with Denture Stomatitis. *J. Oral Pathol. Med.* **2013**, *42*, 698– 704. DOI: 10.1111/jop.12060.

[9] Vinothkumar, S. P.; Murali, K.; Kumar, G. J. Antioxidant Effect of Synthetic Hydroxynaphthoquinone Derivatives. *J. Pharm. Res.* **2010**, *3*, 2784–2787.

[10] Akram, M.; Hamid, A.; Khalil, A.; Ghaffar, A.; Tayyaba, N.; Saeed, A.; Ali, M.; Naveed, A. Review on Medicinal Uses, Pharmacological, Phytochemistry and Immunomodulatory Activity of Plants. *Int. J. Immunopathol. Pharmacol.* **2014**, *27*, 313–319. https://doi.org/10.1177%2F039463201402700301. DOI: 10.1177/039463201402700301.

[11] Lopez-Lopez, L. I.; Nery-Flores, D. S.; Silva-Belmares, Y. S.; Saenz-Galindo, A. Naphthoquinones: Biological Properties and Synthesis of Lawsone and Derivatives - A Structured Review. *Vitae* **2014**, *21*, 248–258.

[12] Singh, D. K.; Luqman, S. Lawsonia inermis (L.): A Perspective on Anticancer Potential of Mehndi/Henna. *Biomed. Res. Ther.* **2014**, *1*, 112–120.

[13] Bustamante, F. L.; Metello, J. M.; De Castro, F. A.; Pinheiro, C. B.; Pereira, M. D.; Lanznaster, M. Lawsone Dimerization in Cobalt(III) Complexes toward the Design of New Prototypes of bioreductive prodrugs. *Inorg. Chem.* **2013**, *52*, 1167–1169. DOI: 10.1021/ic302175t.

[14] Oramas-Royo, S.; Torrejón, C.; Cuadrado, I.; Hernández-Molina, R.; Hortelano, S.; Estévez-Braun, A.; de Las Heras, B. Synthesis and Cytotoxic Activity of Metallic

Complexes of Lawsone. *Bioorg. Med. Chem.* **2013**, *21*, 2471–2477. DOI: 10.1016/j.bmc.2013.03.002.

[15] Mildvan, A. S.; Cohn, M. Kinetic and Magnetic Resonance Studies of the Pyruvate Kinase Reaction. II. Complexes of Enzyme, Metal, and Substrates. *J. Biol. Chem.* **1996**, *241*, 1178–1193.

[16] Tetteh, S.; Dodoo, D. K.; Appiah-Opong, R.; Tuffour, I. Tuffour, I. Spectroscopic Characterization, in Vitro Cytotoxicity, and Antioxidant Activity of Mixed Ligand Palladium(II) Chloride Complexes Bearing Nucleobases. *Inorg. Chem.* **2014**, *2014*, 1–6138. DOI: 10.1155/2014/586131.

[17] Bouwman, E.; Driessen, W. L.; Reedijk, J. Model Systems for Type I Copper Proteins: structures of Copper Coordination Compounds with Thioether and Azole-Containing Ligands. *Coord. Chem. Rev.* **1990**, *104*, 143–172. https://doi.org/10.1016/0010-8545. (90)80042-R. DOI: 10.1016/0010-8545(90)80042-R.

[18] Rajesh, J.; Gubendran, A.; Rajagopal, G.; Athappan, P. Synthesis, Spectra and DNA Interactions of Certain Mononuclear Transition Metal(II) Complexes of Macrocyclictetraazadiacetylcurcumin Ligand. *J. Mol. Struct.* **2012**, *1010*, 169–178. DOI: 10.1016/j.molstruc.2011.12.002.

[19] Kareem, A.; Shoeb Khan, M.; Nami, S. A. A.; Bhat, S. A.; Mirza, A. U.; Nishat, N. Curcumin Derived Schiff Base Ligand and Their Transition Metal Complexes: Synthesis, Spectral Characterization, Catalytic Potential and Biological Activity. *J. Mol. Struct.* **2018**, *1167*, 261–273. DOI: 10.1016/j.molstruc.2018.05.001.

[20] Meza-Morales, W.; Estevez-Carmona, M. M.; Alvarez-Ricardo, Y.; Obregon-Mendoza, M. A.; Cassani, J.; Ramirez-Apan, M. T.; Escobedo-Martíne, C.; Soriano-Garcia, M.; Reynolds, W. F.; Enriquez, R. G. Full Structural Characterization of Homoleptic Complexes of Diacetylcurcumin with Mg, Zn, Cu, and Mn: Cisplatin-Level Cytotoxicity *Invitro* with Minimal Acute Toxicity *Invivo*. *Molecules* **2019**, *24*, 1598. DOI: 10.3390/molecules24081598.

[21] Suganthi, M.; Elango, K. P. Spectroscopic and Molecular Docking Studies on the Albumin-Binding Properties of Metal(II) Complexes of Mannich Base Derived from Lawsone. *J. Biomol. Struct. Dyn.* **2019**, *37*, 1136–1145. DOI: 10.1080/07391102.2018.1450788.

[22] Oliveira, K. M.; Liany, L. D.; Correa, R. S.; Deflon, V. M.; Cominetti, M. R.; Batista, A. A. Selective Ru(II)/Lawsone Complexes Inhibiting Tumor Cell Growth by Apoptosis. *J. Inorg. Biochem.* **2017**, *176*, 66–76. DOI: 10.1016/j.jinorgbio.2017.08.019.

[23] Wadood, A.; Ahmed, N.; Shah, L.; Ahmad, A.; Hassan, H.; Shams, S. *In-Silico* Drug Design: An Approach Which Revolutionarised the Drug Discovery Process. *QA Drug Des. Deliv.* **2013**, *3*, 1–4.

[24] Porkodi, J.; Raman, N. Synthesis, Characterization and Biological Screening Studies of Mixed Ligand Complexes Using Flavonoids as Precursors. *App. Organomet. Chem.* **2018**, *32*, e4030. DOI: 10.1002/aoc.4030..

[25] Gaber, M.; El-Wakiel, N.; El-Baradie, K.; Hafez, S. Chromone Schiff Base Complexes: Synthesis, Structural Elucidation, Molecular Modeling, Antitumor, Antimicrobial, and DNA Studies of Co(II), Ni(II), and Cu(II) Complexes. *J. Iran. Chem. Soc.* **2019**, *16*, 169–182. DOI: 10.1007/s13738-018-1494-9.

[26] Geary, W. J. The Use of Conductivity Measurements in Organic Solvents for the Characterisation of Coordination Compounds. *Coord. Chem. Rev.* **1971**, *7*, 81–122. https://doi.org/10.1016/S0010-8545. (00)80009-0. DOI: 10.1016/S0010-8545(00)80009-0.

[27] Ammar, R. A.; Alaghaz, A.-N. M. A.; Zayed, M. E.; Al-Bedair, L. A. Synthesis, Spectroscopic, Molecular Structure, Antioxidant, Antimicrobial and Antitumor Behavior of Mn(II), Co(II), Ni(II), Cu(II) and Zn(II) Complexes of O_2N Type Tridentate Chromone-2-Carboxaldehyde Schiff's Base Ligand. *J. Mol. Struct.* **2017**, *1141*, 368–381. DOI: 10.1016/j.molstruc.2017.03.080.

[28] Raman, N.; Pothiraj, K.; Baskaran, T. DNA Interaction, Antimicrobial, Electrochemical and Spectroscopic Studies of Metal(II) Complexes with Tridentate Heterocyclic Schiff Base Derived from 2′-Methylacetoacetanilide. *J. Mol. Struct.* **2011**, *1000*, 135–144. DOI: 10.1016/j.molstruc.2011.06.006.

[29] El-Gammal, O. A.; Rakha, T. H.; Metwally, H. M.; Abu El-Reash, G. M. Synthesis, Characterization, DFT and Biological Studies of Isatinpicolinohydrazone and Its Zn(II), Cd(II) and Hg(II) Complexes. *Spectrochim. Acta A. Mol. Biomol. Spectrosc.* **2014**, *127*, 144–156. DOI: 10.1016/j.saa.2014.02.008.

[30] Kavitha, B.; Sravanthi, M.; Saritha Reddy, P. DNA Interaction, Docking, Molecular Modelling and Biological Studies of o-Vanillin Derived Schiff Base Metal Complexes. *J. Mol. Struct.* **2019**, *1185*, 153–167. DOI: 10.1016/j.molstruc.2019.02.093.

[31] Adly, O. M. I.; Ei-Shafiy, H. F. New Metal Complexes Derived from S-Benzyldithiocarbazate (SBDTC) and Chromone-3-Carboxaldehyde: Synthesis, Characterization, Antimicrobial, Antitumor Activity and DFT Calculations. *J. Coord. Chem.* **2019**, *72*, 1–16. DOI: 10.1080/00958972.2018.1564912..

[32] Burgos-Lopez, Y.; Del Pla, J.; Balsa, L. M.; Leon, I. E.; Echeverria, G. A.; Piro, O. E.; García-Tojal, J.; Pis-Diez, R.; Gonzalez-Baro, A. C.; Parajon-Costa, B. S. Synthesis, Crystal Structure and Cytotoxicity Assays of a Copper(II) Nitrate Complex with a Tridentate ONO Acylhydrazone Ligand: spectroscopic and Theoretical Studies of the Complex and Its Ligand. *Inorganica Chim. Acta* **2019**, *487*, 31–40. DOI: 10.1016/j.ica.2018.11.039.

[33] Jagtap, S. B.; Patil, N. N.; Kapadnis, B. P.; Kulkarni, B. A. Characterization and Antimicrobial Activity of Erbium(III) Complexes of C-3 Substituted 2-Hydroxy-1,4-Naphthalenedione-1-Oxime Derivatives. *Met. Based Drugs.* **2001**, *8*, 159–164. DOI: 10.1155/MBD.2001.159.

[34] Speier, G.; Csihony, J.; Whalen, A. M.; Pierpont, C. G. Studies on Aerobic Reactions of Ammonia/3,5-Di-Terf-Butylcatechol Schiff-Base Condensation Products with Copper, Copper(I), and Copper(II). Strong Copper(II)-Radical Ferromagnetic Exchange and Observations on a Unique N-N Coupling Reaction. *Inorg. Chem.* **1996**, *35*, 3519–3524. DOI: 10.1021/ic950805l.

[35] Kamalakannan, P.; Venkappayya, D. Spectral, Thermal, and Antimicrobial Studies on the Copper(II), Zinc(II), Cadmium(II), and Mercury(II) Chelates of a New Antimetabolite–5-Dimethylaminomethyl-2-Thiouracil. *Russ. J. Coord. Chem.* **2002**, *28*, 423–433. https://doi.org/10.1023/A. :1016032928816. DOI: 10.1023/A:1016032928816.

[36] Dudley, R. J.; Hathaway, B. Single-Crystal Electronic and Electron Spin Resonance Spectra of 2,2′-Bipyridylbis(Hexafluoroacetylacetonato)Copper(II). *J. Chem. Soc. A* **1970**, *0*, 2794–2799. DOI: 10.1039/J19700002794.

[37] Sonmez, M.; Celebi, M.; Yardim, Y.; Senturk, Z. Palladium(II) and Platinum(II) Complexes of a Symmetric Schiff Base Derived from 2,6,Diformyl-4-Methylphenol with N-Aminopyrimidine: Synthesis, Characterization and Detection of DNA Interaction by Voltammetry. *Eur. J. Med. Chem.* **2010**, *45*, 4215–4220. DOI: 10.1016/j.ejmech.2010.06.016..

[38] Li, Q. S.; Yang, P.; Wang, H. F.; Guo, M. L. Diorganotin(IV) Antitumor Agent. $(C_2H_5)_2SnCl_2$ (Phen)/Nucleotides Aqueous and Solid-State Coordination Chemistry and Its DNA Binding Studies. *J. Inorg. Biochem.* **1996**, *64*, 181–195. doi.org/DOI: 10.1016/0162-0134(96)00039-6.

[39] Patel, K.; Plummer, A.; Darwish, M.; Rodger, A.; Hannon, J. Aryl Substituted Ruthenium Bis-Terpyridine Complexes: Intercalation and Groove Binding with DNA. *J. Inorg. Biochem.* **2002**, *91*, 220–229. doi.org/DOI: 10.1016/s0162-0134(01)00423-8.

[40] Friedman, A. E.; Chambron, J. C.; Sauvage, J. P.; Turro, N. J.; Barton, J. K. A Molecular Light Switch for DNA: $Ru(Bpy)_2(Dppz)^{2+}$. *J. Am. Chem. Soc.* **1990**, *112*, 4960–4962. doi.org/ DOI: 10.1021/ja00168a052.

[41] Fairley, T. A.; Richard Tidwell, R.; Donkor, I.; Naima, A. N.; Kwari, A.; Ohemeng, A.; Lombardy, R. J.; Bentley, J. A.; Cory, M. Structure, DNA Minor Groove Binding, and Base Pair Specificity of Alkyl- and Aryl-Linked Bis(Amidinobenzimidazoles) and Bis(Amidinoindoles). *J. Med. Chem.* **1993**, *36*, 1746–1753. doi.org/10.1021/jm00064a008. DOI: 10.1021/jm00064a008.

[42] Sundaravadivel, E.; Reddy, G. R.; Manoj, D.; Rajendran, S.; Kandaswamy, M.; Janakiraman, M. DNA Binding and Cleavage Studies of Copper(II) Complex Containing N_2O_2 Schiff Base Ligand. *Inorganica Chim. Acta.* **2018**, *482*, 170–178. DOI: 10.1016/j.ica.2018.06.002.

[43] Tweedy, B. G. Plant Extracts with Metal Ions as Potential Antimicrobial Agents. *Phytopathology* **1964**, *55*, 910–918.

[44] Lipinski, C. A.; Lombardo, F.; Dominy, B. W.; Feeney, P. J. Experimental and Computational Approaches to Estimate Solubility and Permeability in Drug Discovery and Development Settings. *J. Adv. Drug. Deli. Rev.* **2001**, *46*, 3–25. doi.org/ DOI: 10.1016/S0169-409X(96)00423-1.

[45] Veber, D. F.; Johnson, S. R.; Chen, H. Y.; Smith, B. R.; Ward, K. W.; Kopple, K. D. Molecular Properties That Influence the Oral Bioavailability of Drug Candidates. *J. Med. Chem.* **2002**, *45*, 2615–2623. doi.org/10.1021/jm020017n. DOI: 10.1021/jm020017n.

[46] Chaudhary, M.; Kumar, N.; Baldi, A.; Chandra, R.; Babu, M. A.; Madan, J. 4-Bromo 4'-Chloro Pyrazoline Analog of Curcumin Augmented Anticancer Activity against Human Cervical Cancer, HeLa Cells: *In-Silico* Guided Analysis, Synthesis and in-Vitro Cytotoxicity. *J. Biomol. Struct. Dyn.* **2020**, *38*, 1335–1353. DOI: 10.1080/07391102.2019.1604266.

[47] Parashar, R. K.; Sharma, R. C.; Kumar, A.; Mohan, G. Stability Studies in Relation to IR Data of Some Schiff Base Complexes of Transition Metals and Their Biological and Pharmacological Studies. *Inorganica Chim. Acta* **1988**, *151*, 201–208. DOI: 10.1016/S0020-1693(00)83468-4.

[48] Leung, C.; Lin, S.; Zhong, H.; Ma, D. Metal Complexes as Potential Modulators of Inflammatory and Autoimmune Responses. *Chem. Sci.* **2015**, *6*, 871–884. DOI: 10.1039/c4sc03094j.

[49] Hoonur, R. S.; Patil, B. R.; Badiger, D. S.; Vadavi, R. S.; Gudasi, K. B.; Dandawate, P. R.; Ghaisas, M. M.; Padhye, S. B.; Nethaji, M. Transition Metal Complexes of 3-Aryl-2-Substituted 1,2-Dihydroquinazolin-4(3H)-One Derivatives: New Class of Analgesic and anti-Inflammatory Agents. *Eur. J. Med. Chem.* **2010**, *45*, 2277–2282. DOI: 10.1016/j.ejmech.2010.01.072.

[50] Kendur, U.; Chimmalagi, G. H.; Patil, S. M.; Gudasi, K. B.; Frampton, C. S.; Mangannavar, C. V.; Muchchandi, I. S. Mononuclear Late First Row Transition

Metal Complexes of ONO Donor Hydrazone Ligand: Synthesis, Characterization, Crystallographic Insight, *in Vivo* and *in Vitro* Anti-Inflammatory Activity. *J. Mol. Struct.* **2018**, *1153*, 299–310. doi.org/ DOI: 10.1002/aoc.4557.

[51] Vanhaecke, P.; Persoone, G.; Claus, C.; Sorgeloos, P. Proposal for a Short-Term Toxicity Test with Artemia nauplii. *Ecotoxicol. Environ. Saf.* **1981**, *5*, 382–387. doi.org/10.1016/0147-6513(81)90012-9. DOI: 10.1016/0147-6513(81)90012-9.

[52] Meyer, B. N.; Ferrigni, N. R.; Putnam, J. E.; Jacobsen, L. B.; Nichols, D. E.; McLaughlin, J. L. Brine Shrimp: A Convenient General Bioassay for Active Plant Constituents. *Planta Med.* **1982**, *45*, 31–34. DOI: 10.1055/s-2007-971236.

[53] Hobani, Y.; Jerah, A.; Bidwai, A. A Comparative Molecular Docking Study of Curcumin and Methotrexate to Dihydrofolate Reductase. *Bioinformation* **2017**, *13*, 63–66. DOI: 10.6026/97320630013063.